41st Aerospace Sciences Meeting and Exhibit
6-9 January 2003, Reno, Nevada

AIAA 2003-310

LES of Partially-Premixed Unsteady Combustion

C. Stone*and S. Menon†
School of Aerospace Engineering
Georgia Institute of Technology
Atlanta, Georgia, USA 30332
{christopher_stone, suresh.menon}@ae.gatech.edu
http://www.ccl.gatech.edu

Large-Eddy Simulation (LES) methodology has been used to model the combustion dynamics in a realistic swirl-stabilized dump combustor. A novel partially-premixed flamelet combustion model is employed to capture the interaction of the unsteady flame-front with local velocity and equivalence ratio fluctuations. Two sets of simulations have been conducted which employ this combustion model. First, the model is used to simulate temporal variations in the mean inlet fuel flow-rate mimicking pressure and fuel feed-line interaction, a major source of instabilities. The second application models the effects of unmixedness as a result of spatial various in the inlet equivalence ratio. A baseline, uniform equivalence ratio simulation is also reported and is used for comparison. It is shown that the present model is capable of capturing the combustion dynamics under both temporal and spatial fluctuations in the equivalence ratio.

1 Introduction

Due to increasingly stringent emission regulations, clean burning, low NO_x combustion devices are in high demand. To achieve the desired emissions levels, modern combustion devices are being designed to operate in the lean limit. The lower associated combustion temperatures result in suppression of thermal NO_x formation (Zeldovich thermal NO_x mechanism). However, as the equivalence ratio approaches the Lean-Blowout limit (LBO), the sensitivity to small perturbations in fuel concentration, flow velocity, temperature, and pressure increase due to the strong dependence of flame speed on the local equivalence ratio. Under certain conditions, these fluctuations can become self exciting and amplified, resulting in high-amplitude, longitudinal pressure oscillations. Structural fatigue, increased combustor core noise and/or possible system failure could result if these oscillations are not controlled.

Nearly all operational gas turbine combustors employ swirl stabilization of the combustion process since the swirl-induced Vortex-Breakdown (VB) phenomena (i.e., axial flow-reversal) provides a natural mechanism for flame stabilization. Typically, swirl is introduced by a premixer that is located upstream of the combustor and consists of many angled vanes (e.g. the Dual Annular Counter-Rotating Swirlers (DACRS)[1]). Several studies in recent years have dealt with swirl stabilized combustion either experimentally[2] or numerically.[3,4] Despite the advantages in swirl-stabilized combustion systems, there still can exist instabilities in the system.

Unsteady combustion may become unstable when perturbations in pressure (p') and heat-release (q') occur in phase (i.e., $|p'\ q'| > 0$). This criterion, known as the *Rayleigh Criterion*, can be viewed based on the volumetric expansion associated with heat-release coupling with that of p'. When this criterion is satisfied, acoustic energy is being added to the system causing an amplification of p'. This amplification then results in a feedback loop and the instabilities have become self-excited.

A combustion instability mechanism often observed in gaseous premixed combustors is based on fluctuations in the incoming equivalence ratio (Φ). This mechanism has been both experimentally[5] and theoretically[6,7] studied in the past. Generally, this mechanism is caused by pressure/velocity fluctuations interacting with fuel feed-lines causing variations in the equivalence ratio (Φ'). Another possible source of fluctuating fuel content is incomplete fuel/air mixing. The resulting fluctuations, which are then convected to the combustion region, can lead to fluctuations in the flame-front location and heat-release (q'). As mentioned earlier, the fluctuations in p' and q' can couple leading to self-excited combustion instabilities. It must be noted that it is possible and is highly likely that multiple instability mechanism exist in a single combustion system. Another important instability source is vortex-flame interaction which, coupled with incomplete mixing, can lead to highly unstable combustion.

The focus of this article is on numerically modelling spatial and temporal variations in the local equivalence ratio and their qualitative and quantitative effects on the stability of an idealized, swirl-stabilized gas turbine combustion system. Large-Eddy Simula-

*Student Member, AIAA
†Associate Fellow, AIAA

tion (LES) is used to capture the turbulent combustion dynamics. The theory of LES and a brief background on unsteady turbulence modelling are given in the next section. This is followed by details of the numerical model. A brief validation study is then reported to give credence to the combustion model. Finally, results from the three simulations are reported: a baseline, constant equivalence ratio case, a temporal equivalence ratio variation case and a spatial equivalence ratio case.

2 Turbulence Modelling Background

In the past, combustion system designers have relied heavily upon low-order empirical and, to a lesser extent, physical models for performance, emission, and stability predictions. Due to the lack of sufficient computational power, modelers were forced to make sometimes sweeping assumptions and simplifications about the highly-coupled and complex combustion processes. The turbulent nature of the flows inside most practical combustion devices makes modelling even more difficult. In the past and even at present, multi-dimensional modelling of combustion systems employing CFD has been largely limited to steady-state analysis. However, most physical processes occurring in a gas turbine combustor are naturally dynamic or unsteady (e.g., pressure oscillations).

In turbulent flows, kinetic energy is transferred from larger to smaller scales until it finally reaches a scale at which molecular viscosity dominates (and where kinetic energy is converted to thermal energy). This so-called *energy cascade* from large to small scales is a fundamental nature of turbulence (the smallest scale is known as the Kolmogorov micro-scale (η)). The dynamics of turbulent flow at the different length scales are quite different. Large-scale fluctuations are caused by large eddies, often referred to "coherent-structures". These eddies, which contain most of the kinetic energy, are controlled by the geometry of the system and are generally an-isotropic while small scales, which receive their energy from the larger scales, are isotropic and more universal. It is, therefore, critical that the dynamics of the large scale turbulent motion is resolved to capture the unsteady dynamics.

Although DNS of real-world devices is not possible, a relatively newer modelling technique, known as Large-Eddy Simulation (LES), is becoming feasible. In LES, turbulent fluctuations smaller than the local grid volume (known as *sub-grid scales* (*SGS*)) are modelled while all larger scales are fully resolved in space and time. Since the large eddy dynamics are fully resolved, a realistic representation of part of the turbulent field is possible. It should be noted that the accuracy of LES is dependent not only on the resolution of the large eddies but also on the fidelity of the *SGS* models used to characterize the small-scale effects. Unlike steady-state modelling methods, LES is capable of capturing unsteady combustion phenomena such as combustion instabilities and has, therefore, garnered attention as a next-generation design tool. Even with the dramatic savings offered by LES over DNS, the use of LES to study complex systems is still an expensive proposition, often requiring 1000's of hours of computation. However, through the use of massively parallel computers, the time-to-solution can be dramatically reduced.

3 Formulation and Numerical Implementation

For this study, a parallel simulation model based on LES is used to model the flow inside a realistic gas-turbine combustor. Details of the algorithm are divided into distinct sections: (1) the governing conservation equations, (2) LES sub-grid closure, (3) combustion model and (4) numerical implementation.

3.1 Governing conservation equations

The unsteady, compressible Navier-Stokes equations govern the flow of current interest. Employing tensor notation, the conservation equation for mass, momentum, and energy are, respectively:

$$\begin{aligned} \frac{\partial \rho}{\partial t} &= -\frac{\partial \rho u_i}{\partial x_i} \\ \frac{\partial \rho u_i}{\partial t} &= -\frac{\partial}{\partial x_j}[\rho u_i u_j + p\delta_{ij} - \tau_{ij}] \\ \frac{\partial \rho E}{\partial t} &= -\frac{\partial}{\partial x_i}[\rho H u_i + q_i - u_j \tau_{ji}] \end{aligned} \tag{1}$$

where ρ is the mass density, p is the pressure, E is the total energy per unit mass, u_i is the velocity vector, q_i is the heat flux vector, τ_{ij} is the viscous stress tensor and H is the total enthalpy per unit mass. These equations are completed with the following relations:

$$\begin{aligned} \tau_{ij} &= \mu\,(\frac{\partial u_i}{\partial x_j} + \frac{\partial u_j}{\partial x_i}) - \frac{2}{3}\,\mu\,\frac{\partial u_k}{\partial x_k}\,\delta_{ij} \\ q_i &= -\kappa\,\frac{\partial T}{\partial x_i} \\ p &= \rho\,R\,T \\ E &= C_v\,T + \frac{1}{2}\,u_k^2 \\ H &= (E+p)\,/\,\rho \\ \mu &= \mu_0\,(\frac{T}{T_0})^{3/2}\,\frac{T_0+110}{T+110} \\ \kappa &= \frac{\mu\,C_p}{Pr} \end{aligned} \tag{2}$$

Here, μ, κ, C_p, and Pr are, respectively, the molecular viscosity (approximated by Sutherland's Law), the thermal conductivity, the specific heat at pressure and the Prandtl number ($Pr = 0.72$ for air).

These equations can be treated as an exact mathematical model for the motion of perfect gases regardless of whether or not the flow is laminar or highly turbulent. However, DNS resolution is required to exactly recover the equations in a computational model. As this is not practical, a LES representation of the governing equations is therefore needed.

As briefly mentioned earlier, LES fully resolves the large-scale dynamics and employs models at the sub-grid level. Therefore, an operation is required which can separate or *filter* the governing Navier-Stokes equations into large-scale and *SGS* components. This is achieved, following Erlebacher *et al.*,[8] by applying a spatial filtering operation to the governing equations such that $f = \widetilde{f} + f''$. There, $\sim$ and $''$ denote the resolved super-grid and unresolved sub-grid quantities, respectively. The resolved super-grid quantities are determined by Favre filtering: $\widetilde{f} = \overline{\rho f}/\overline{\rho}$ where the over-bar represents spatial filtering defined as

$$\overline{f(x_i,t)} = \int f(x_i',t) G_f(x_i,x_i') dx_i'. \tag{3}$$

Here, G_f is the filter kernel and the integral is over the entire computational domain. Applying this filtering operation (basically, a low-pass filter of local grid size $\overline{\Delta}$) to the Navier-Stokes equations, the following LES equations are obtained:

$$\begin{aligned}
\frac{\partial \overline{\rho}}{\partial t} &= -\frac{\partial \overline{\rho}\widetilde{u}_i}{\partial x_i} \\
\frac{\partial \overline{\rho}\,\widetilde{u}_i}{\partial t} &= -\frac{\partial}{\partial x_j}[\overline{\rho}\widetilde{u}_i\widetilde{u}_j + \overline{p}\,\delta_{ij} - \overline{\tau}_{ij} + \tau_{ij}^{sgs}] \\
\frac{\partial \overline{\rho}\widetilde{E}}{\partial t} &= -\frac{\partial}{\partial x_i}[\overline{\rho}\widetilde{H}\widetilde{u}_i + \overline{q}_i - \widetilde{u}_j\overline{\tau}_{ji} + H_i^{sgs} + \sigma_{ij}^{sgs}]
\end{aligned} \tag{4}$$

The sub-grid terms resulting from the filtering operation, denoted with super-script ^{sgs}, represent the small-scale effects upon the resolved-scales in the form of additional stresses and fluxes. The filtered velocity, $\widetilde{u}_i$, and temperature, $\widetilde{T}$, are used to approximate $\overline{\tau}_{ij}$ and $\overline{q}_i$, respectively. The resulting *SGS* terms, the sub-grid stress tensor, sub-grid heat flux, and unresolved viscous work are defined, respectively, as:

$$\begin{aligned}
\tau_{ij}^{sgs} &= \overline{\rho}\,[\widetilde{u_i u_j} - \widetilde{u}_i\widetilde{u}_j] \\
H_i^{sgs} &= \overline{\rho}\,[\widetilde{Eu_i} - \widetilde{E}\widetilde{u}_i] + [\overline{pu_i} - \overline{p}\widetilde{u}_i] \\
\sigma_i^{sgs} &= [\overline{u_j\tau_{ij}} - \widetilde{u}_j\overline{\tau}_{ij}].
\end{aligned} \tag{5}$$

3.2 LES sub-grid closure

The sub-grid terms, Eqn. 5, require explicit modelling since the small-scale correlations are not known. Generally, these models require some form of sub-grid velocity and length scale for closure. For this study, the *SGS* velocity field is calculated from the modelled sub-grid turbulent kinetic energy (the kinetic energy not captured on the super-grid). The sub-grid characteristic length scale is modelled as the local grid size, $\overline{\Delta}$ $(= (\Delta x_1 \Delta x_2 \Delta x_3)^{1/3}$, i.e., the cube-root of the local grid volume). A transport equation for the sub-grid kinetic energy, defined as $k^{sgs} = \frac{1}{2}[\widetilde{u_k^2} - \widetilde{u}_k^2]$, was derived by Menon *et al.*:[9]

$$\begin{aligned}
\frac{\partial \overline{\rho}\,k^{sgs}}{\partial t} \;+\; \frac{\partial}{\partial x_i}\left(\overline{\rho}\,\widetilde{u}_i k^{sgs}\right) \;&=\; \\
P^{sgs} \;-\; D^{sgs} \;+\; \tfrac{\partial}{\partial x_i}&\left(\overline{\rho}\,\tfrac{\nu_t}{Pr_t}\tfrac{\partial k^{sgs}}{\partial x_i}\right).
\end{aligned} \tag{6}$$

were Pr_t is the turbulent Prandtl number which is assumed constant and equal to unity. P^{sgs} and D^{sgs} are, respectively, the production and dissipation of k^{sgs}. The production term is defined as, $P^{sgs} = -\tau_{ij}^{sgs}(\partial\widetilde{u}_i/\partial x_j)$, where τ_{ij}^{sgs} is the modelled sub-grid stress tensor,

$$\tau_{ij}^{sgs} = -2\,\overline{\rho}\,\nu_t\,(\widetilde{S}_{ij} - \frac{1}{3}\,\widetilde{S}_{kk}\delta_{ij}) + \frac{2}{3}\,\overline{\rho}k^{sgs}\delta_{ij}, \tag{7}$$

where $\nu_t = C_\nu (k^{sgs})^{1/2}\overline{\Delta}$ is the eddy viscosity and $\widetilde{S}_{ij}, = \frac{1}{2}(\partial\widetilde{u}_i/\partial x_j + \partial\widetilde{u}_j/\partial x_i)$ is the resolved rate-of-strain tensor. The dissipation term is modelled as $D^{sgs} = C_\varepsilon\overline{\rho}(k^{sgs})^{3/2}/\overline{\Delta}$. The coefficients, C_ν and C_ε can be assumed constant (set to 0.067 and 0.916, respectively based on a study by Chakravarthy and Menon[10]), or can be dynamically determined by using a Localized Dynamic k-equation Model (LDKM) proposed by Kim and Menon.[3]

Finally, the sub-grid heat-flux, H_i^{sgs}, is modelled as,

$$H_i^{sgs} = -\overline{\rho}\frac{\nu_t}{Pr_t}\frac{\partial\widetilde{H}}{\partial x_i}, \tag{8}$$

and the sub-grid viscous work may be modelled as $\sigma_i^{sgs} = \widetilde{u}_j\tau_{ij}^{sgs}$. However, σ_i^{sgs} is neglected in the present study based on the earlier work of Kim *et al.*[11]

3.3 Combustion model

The previous sections have treated the gas as a single species without any chemical reactions. However, to simulate the combustion of interest, chemical reactions must be explicitly included. Detailed finite-rate chemical kinetics in LES can be very expensive due to the wide range of chemical time-scales. Fortunately, an alternate, computationally efficient approach exists for premixed and partially-premixed combustion. A premixed flame at moderate turbulent levels can be modelled as a thin surface which is convected and contorted by the local velocity fluctuations. This assumption is valid so long as the flame thickness (δ) is much smaller than η (previously defined turbulent micro-scale) and the burning time-scale is small compared to that of the turbulence. Under these assumptions, the flame remains locally laminar and its burning velocity (directed normal to the surface) is

balanced by the local flow. Extensive literature exists on such flame surface models (also known as *flamelet* models), see Peters[12] for more details. As opposed to directly solving a set of N chemical reactions (and N additional conservation equations which are generally quite stiff), premixed *flamelet* models require the solution of only a single scalar field. Obviously this can reduce the computational expense. *Flamelet* models, however, cannot directly predict pollutant emissions or flame extinction since no chemistry is involved; but, they do provide accurate prediction of unsteady heat release and flame-turbulence interactions. Therefore, this flamelet model is used to study combustion dynamics which is interest here.

Following Williams[13] and Kerstein *et al.*,[14] a model equation that describes the convection and propagation of a thin, laminar flame is the G-equation. The G-equation, in conservative form, can be written as:

$$\frac{\partial \rho G}{\partial t} + \frac{\partial \rho u_i G}{\partial x_i} = -\rho S_L |\nabla G| \tag{9}$$

where G is a scalar variable defining the flame location and S_L is the laminar burning velocity of the flame (flame speed). The scalar field G is defined in the region [0,1] in which the unburnt products are assigned $G = 1$ and hot, reacted gases are $G = 0$. The flame surface is defined as an iso-scalar surface, G_0 ($0 < G_0 < 1$). Essentially, this models a level-surface, at $G = G_0$, being convected by the local flow-field and propagating at S_L. All chemical and diffusive processes are implicitly included in S_L and, therefore, no specific species transport needs to be modelled.

Applying the same spatial filtering operation as before, Eqn. 9 can be adapted for the LES formulation. The resulting filtered G-equation[15] and resulting SGS terms are:

$$\frac{\partial \overline{\rho}\widetilde{G}}{\partial t} + \nabla \cdot \overline{\rho}\tilde{u}\widetilde{G} = -S^{sgs} - \nabla \cdot G^{sgs}. \tag{10}$$

The two sub-grid terms, S^{sgs} and G^{sgs}, are, respectively, the filtered source and the unresolved transport. G^{sgs} is closed, in similar fashion to H_i^{sgs}, by assuming a sub-grid fluctuations act as a diffusive process in the direction of the resolved-scale gradient, i.e. $G^{sgs} \approx -\frac{\overline{\rho}\nu_t}{Sc_t}\nabla\widetilde{G}$ (Sc_t is the turbulent Schmidt number, a ratio of viscous to chemical diffusion rates). An alternate closure method for G^{sgs} focuses on the flame-curvature.[12] With this method, G^{sgs} is approximated as $-\frac{\overline{\rho}\nu_t}{Sc_t}k|\nabla\widetilde{G}|$, where k is the resolved flame curvature, $\nabla \cdot \nabla\widetilde{G}/|\nabla\widetilde{G}|$. As will be shown later, the performance of the two models is quite similar with the only major differences being their respective computational expense. The former model, being less expensive, will therefor be used for this study. The unresolved source term is modelled as $S^{sgs} \approx \rho_0 S_t |\nabla\widetilde{G}|$, where S_t, is the local turbulent flame speed averaged over a characteristic LES cell. For the present study, Pocheau's flame speed model[16] has been used to determine the turbulent flame speed in the following form;

$$\frac{S_t}{S_L} = (1 + \beta\frac{u'^{\alpha}}{S_L^{\alpha}})^{\frac{1}{\alpha}}. \tag{11}$$

where u' is the unresolved fluctuating velocity calculated from k^{sgs}, $u' = \sqrt{\frac{2}{3}k^{sgs}}$. Following Kim *et al.*,[11] α and β are taken as 2 (based on energy conservation) and 20, respectively.

In order to account for local variations in the local fuel composition (i.e., partially-premixed combustion regime), the G-equation must be augmented by a second scalar equation tracking the local mixture fraction, Z. This equation takes following form in LES:

$$\frac{\partial \overline{\rho}\widetilde{Z}}{\partial t} + \nabla \cdot [\overline{\rho}\tilde{u}\widetilde{Z} - \rho D \nabla\widetilde{Z}] = -\nabla \cdot Z^{sgs}. \tag{12}$$

where Z^{sgs} is closed with a common gradient diffusion model. A benefit of this model this the lack of reaction source terms in Eqn. 12 makeing this model inexpensive.

For uniform equivalence ratio, heat-release is introduced into the systems by coupling G to the super-grid internal energy,

$$E_i = C_v\ T + C_p\ (T_f - T_0)\ \widetilde{G}, \tag{13}$$

where T_f and T_0 are the temperatures of the products and reactants, respectively. For non-uniform equivalence ratio, Eqs. 11 and 13 must be adjusted. This case, the value of S_L and T_f are no longer constant but are functions of $\widetilde{Z}$. The functional dependency can be seen in Fig. 1 where both S_L and T_f have been plotted against Z. These results where obtained from the CHEMKIN software package.[17,18] In their modified forms, S_L and T_f in Eqs. 11 and 13, respectively are replaced by $S_L(Z)$ and $T_f(Z)$. The closure of the turbulent burning rate is not changed for this study which limits the current model to only mild or large-scale fluctuations in the local mixture fraction and that the mixture remain lean (i.e., $\Phi < 1$). However, for the present study, which is focused on large-scale temporal/spatial variations in Φ, this should not be a major issue.

3.4 Numerical method

The governing LES equations are solved using a finite-volume formulation in which the integral form of Eqn. 4 are integrated over a discrete control-volumes. An explicit, second-order accurate in time and fourth-order in space *Predictor-Corrector*[19,20] scheme is used. In this scheme, two one-sided, second-order accurate differences are combined to give an overall fourth-order accurate formulation. A non-uniform, boundary-conforming computational grid is

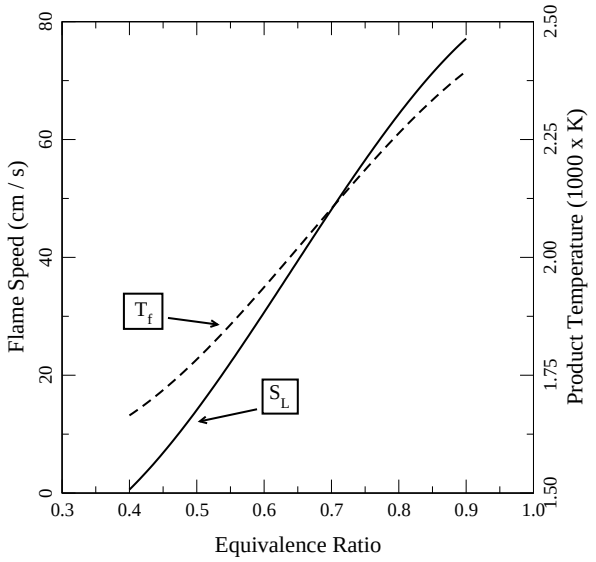

Fig. 1 Flame speed (S_L) and product temperature (T_f) dependence on mixture fraction/equivalence ratio (Z/Φ). Solid and dashed line show S_L and T_f relationships, respectively.

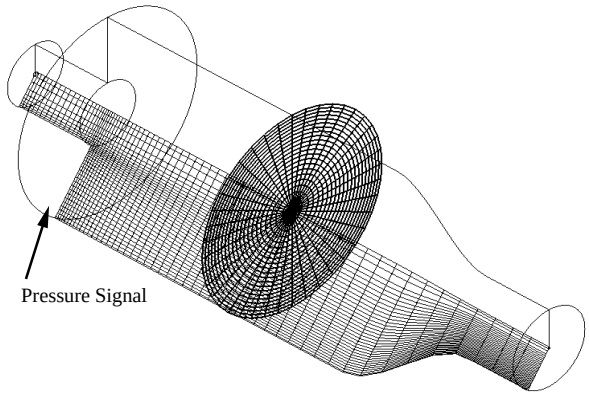

Fig. 2 Geometry and computational grid (181 × 73 × 81), only every third grid point is shown. Acoustic signals are recorded at the base of the combustor.

used to account for the complex geometry. This requires the governing equations, written in Cartesian coordinates, to be recast in generalized curvilinear coordinates (i.e., $\phi(x, y, z) = \phi(\xi, \eta, \zeta)$). In regions of high spatial gradients (turbulent shear layers, combustion zone, etc.), the grid is concentrated to more accurately capture the physical phenomena. It must be noted that non-uniformities on the computational grid reduce the numerical accuracy; however, efforts are taken to minimize this effect.

Fig. 2 shows the computational grid used to model the unsteady flow inside a cylindrical, gas-turbine combustor. The small pipe represents the combustor inlet and the larger chamber is the actual combustor. The converging region is the exhaust port. At the solid boundaries of the combustor, the heat-flux and the transverse and normal velocity are set to zero (i.e., adiabatic, no-slip, zero-penetration conditions). Finally, acoustically non-reflecting boundary conditions are applied at the free boundaries following Poinsot and Lele.[21]

In order to achieve results in a reasonable timeframe, large-scale parallel computing has been employed. For the LES algorithm used here, the computational grid is partitioned and distributed evenly among the available processors in the distributed computing system. This parallel decomposition method is well suited for problems such as this since it allows for easy scalability with increasing problem size. To make the LES algorithm portable, the standardized Message-Passing Interface (MPI) protocol is used for parallel communication.

4 Model Configuration

For this study, a generic swirling dump combustor is simulated. The geometry consists of a straight inlet duct expanding suddenly into the larger combustion zone. The ratio of the combustor diameter to the inlet diameter, D_0, is 3.2. The inlet length is 1.25 D_0 and the combustor is 5.5 D_0. A swirling velocity profile is specified at the inlet and allowed to evolve towards the dump plane. A cylindrical grid of 181 × 73 × 81 (axial, radial, azimuthal directions, respectively) is used (see Fig. 2). The smaller pipe represents the combustor inlet which begins just down-stream of the premixer/swirl-generator. The mean inlet mass flow rate, temperature, and pressure are 0.435 kg/s, 673 K, and 11.8 atm., respectively. The combustor Reynolds number based on the mean inlet bulk velocity, U_0 and D_0 is 527,000.

An common metric of the degree of swirl is the swirl number (S), defined as

$$S = \frac{\int_0^R \rho u w r^2 \mathrm{d}r}{R \int_0^R \rho u^2 r \mathrm{d}r}, \tag{14}$$

where R is the pipe radius. For the present studies, $S = 0.56$. A Gaussian random field (7% of the mean) is added to the inlet velocity profile to mimic inflow turbulence. To wash out the effects of the initial conditions, all simulations are evolved 3–5x the largest time-scale of the system.

5 Results and Discussion

In this section, results from various simulations are presented and, through analysis, their significance noted. The results have been divided into four general sections: (1) model validation results, (2) baseline constant equivalence ratio simulations, (3) time-varying

inlet fuel flow-rate and (4) spatial inlet fuel concentration variation.

5.1 LES premixed combustion validation

Before presenting the main focus of this article, the preformance/accuracy of the present LES algorithm must be assessed. The experimental study of Joshi *et al.*[1] has been chosen for comparison due to its similarity to the current configuration. The combustor configuration is shown in Fig. 3. Unlike the circular combustor of the present study, the experimental rig uses a rectangular geometry; however, the inlet and flame region utilize the same configuration and velocity profiles (with $S = 0.56$). Additionally, cooling jets are placed at the top and bottom walls to allow optical access. Both of these complexities have been included in the numerical model. A relatively coarse grid of 97 x 65 x 81 (axial, radial, azimuthal) is used for this validation study.

Shown in Figs. 4(a)-(c) are the resulting time-averaged velocity profile for both G^{sgs} closure methods previously mentioned in Sec. 3.3. Also plotted in each, is the experimental data from Joshi *et al.*[1] The mean normalized axial velocity ($\overline{U}/\mathrm{U_0}$) along the combustor centerline is shown in Fig. 4(a). As can be seen in the near-field of the inlet, the centerline velocity rapidly decays with increased distance downstream. Between $1.5 < \mathrm{x/D_0} < 2.25$, the centerline velocity becomes negative and the flow stagnates. This phenomena of flow reversal is known as *Vortex Breakdown (VB)* and is a result of an adverse pressure gradient induced by the highly swirling flow (due to force imbalance between outward expulsion of fluid and the axial momentum[22]). Similar results can be seen from both G^{sgs} models and both show reasonable agreement with the available experimental data. In a similar fashion, Fig. 4(b) contains the centerline *rms* axial velocity (u) profile. Again, the two different G^{sgs} closure techniques behave nearly identical with the flame curvature model resulting in slightly higher u. The over-prediction near the inlet may be a results of the random noise superimposed on the mean flow. However, beyond $\mathrm{x/D_0} \approx 0.9$, the agreement is acceptable. Finally, $\overline{U}/\mathrm{U_0}$ is plotted against the radius (r) at $\mathrm{x/D_0} = 0.18$ in Fig. 4(c). There, the structure of swirling jets can be ascertained. Unlike the gaussian profile of non-swirling, turbulent jets, more of the jet momentum is concentrated towards the outer edges. Beyond the swirling jet itself (i.e., $r/\mathrm{D} > 0.5$), the fluid is not completely stagnant as a result of the combustor confinement. Despite a small under-prediction of the spreading rate, the agreement with experiments is again acceptable As with the previous results, the closure of G^{sgs} does not greatly affect the overall mean profiles. Based on these results, it has been concluded that the less costly gradient-diffusion closure of G^{sgs} is sufficient and will be used exclusively for the remainder of the study.

Figs. 5(a) and (b) show a two-dimensional slice of the time-averaged flow-field from the centerline outward to $r/\mathrm{D_0} \approx 1.25$. The extent of the VB region (or bubble) can be seen in Fig. 5(a) where $\overline{U}/\mathrm{U_0}$ has been plotted. The zero-velocity region has been labelled and contour regions with negative velocity are noted with a dashed line. The VB bubble extends radially to $r/\mathrm{D_0} \approx 0.77$ and axially to $r/\mathrm{D_0} \approx 1.22$ (at the greatest). The effect of swirl on the jet spreading can be clearly seen in this figure. The bulk of the jet momentum is directed at an angle towards the upper combustor wall. Downstream, beyond the VB bubble, the momentum is more evenly distributed as can be seen by the increased spacing between the contour lines.

The dynamically evaluated eddy-dissipation coefficient, C_ν, is shown in Fig. 5(b). As can be seen from the contour plot, this coefficient is far from constant (as is often assumed in turbulence modelling), ranging by more than a decade over the flow-field. In regions of high resolution (small $\overline{\Delta}$), such as that found near the inlet and velocity shear-layer, C_ν is indicating that the LES modelling is reduced. Downstream, where the grid is stretched and less refined, the SGS dissipation increases to accommodate. In the core region near the flame, C_ν is close to the typical value of 0.067.

5.2 Baseline simulation

For comparison, a baseline simulation has been conducted with a constant inlet equivalence ratio of $\Phi = 0.52$. At this equivalence ratio, the product temperature (T_f) and laminar flame speed (S_L) are 1812.2 (K) and 17.25 (cm/s), respectively.

Under the current operating conditions, this model combustor is naturally unstable. Coherent, large-scale vortices are shed at the dump plane as a result of acoustic forcing from the resonate acoustic mode. An example of this shedding is shown in Fig. 6. The vortex structures are identified by the λ_2 method.[23] Large-scale, coherent structures (CS) which appear as rings, can be seen entraining the flame surface. As they convect downstream, the rings drag the flame along until they eventually collapse due to vortex stretching. The flame does not propagate indefinitely but retracts toward the combustor inlet plane resulting in a longitudinal pulsation cycle. The flame dynamics are quite similar to that observed by Ducruix *et al.*[24] in a study of forced longitudinal flow perturbations.

Shown in Figs. 7(a)-(d) are various power spectra (in frequency domain) extracted from this simulation. During the course of a simulation, data are recorded through time at various locations within the combustor domain effectively acting as experimental probes. All acoustic signals (pressure, divergence, etc.) reported here were recorded at the base of the combustor (see Fig. 2). In this region, the velocity/vorticity fluctuations are presumed to be small and the resulting

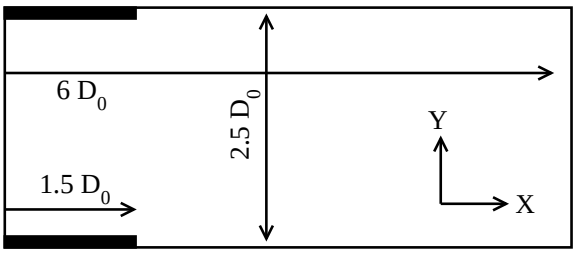

a) xy-plane: mean flow from left to right.

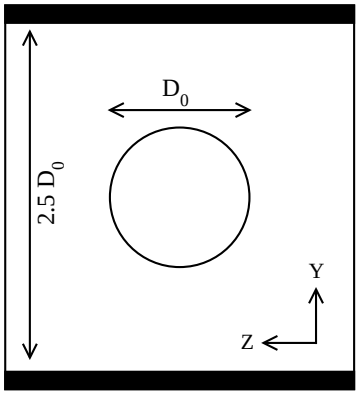

b) yz-plane: mean flow out of page.

Fig. 3 Model configuration for validation studies following Joshi *et al.*[1] In (a), an span-wise view is shown; (b) the yz-plane showing the circular inlet. Blowing sections are shown as filled blocks. All dimensions are normalized by the inlet diameter.

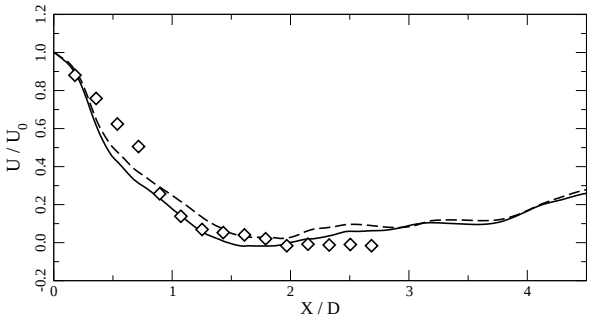

a) $\overline{U}/\mathrm{U}_0$ Centerline Profile

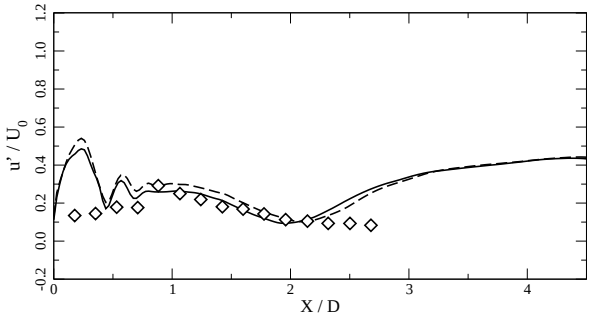

b) u /U_0 Centerline Profile

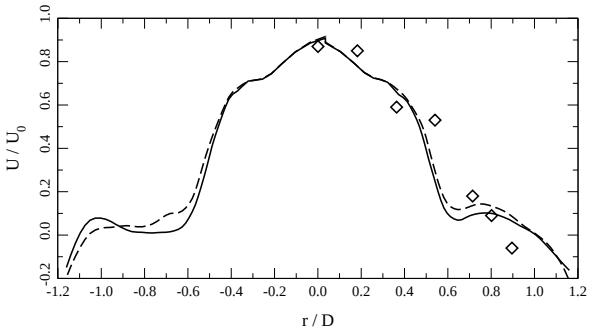

c) $\overline{U}/\mathrm{U}_0$ Radial Profile at $\mathrm{x/D_0} = 0.18$

Fig. 4 Numerical model validation results: Solid lines denote the baseline gradient diffusion algorithm; dashed (- - -) lines denote flame curvature closure; symbols show experimental data from.[1]

pressure fluctuations can be attributed to the acoustic pressure.

The resulting fluctuating pressure (p') and divergence (Δ') have been plotted in Fig. 7(a) and (b), respectively. There, the data has been transformed from the time to the frequency domain by way of a discreet Fourier Transform (DFT). The peak p' frequency occurs at 2918 Hz and the *rms* amplitude normalized by the mean pressure is 1.77%. This corresponds to a sound pressure level of 176 decibels (dB). Similarly, Δ' also shows a dominant peak at 2918 Hz. The matching between the two signals indicates that the fluctuations are acoustically driven, and not resulting from vorticity fluctuations.

Figs. 7(c) and (d) contain the fluctuating of vorticity ($|\omega|'$) and axial velocity (u'). Both of these signals were recorded 1.1 D_0 downstream from the combustor base plane in the velocity shear-layer at $r\ /\ D_0 = 0.6$. As with p' and Δ', u' shows a peak near 3 kHz. In this case, however, the peak frequency has been shifted slightly higher to 3026 Hz. It is speculated that this shift may be attributable to the increased mach number at this specific location. Additionally, this location is in the vicinity of the flame who's temperature gradients may interact with the driving frequency. The *rms* velocity fluctuation at this point in the combustor is 44% of the local mean ($\approx$ 132 m/s). This high level of fluctuation is associated with a strong monopole-like acoustic source (mass surge). Beyond the dominant frequency, the energy decays following the -5/3 scaling law for the inertial range. As previously stated, it is vital to resolve into the inertial range length-scales since these scales contain the vast majority of the turbulent kinetic energy. Finally, the $|\omega|'$ spectrum contains the same dominant frequency in addition to a harmonic peak at 6 kHz (associated with vortex-pairing). The 3 kHz frequency corresponds to the vortex passage frequency (i.e., shedding rate).

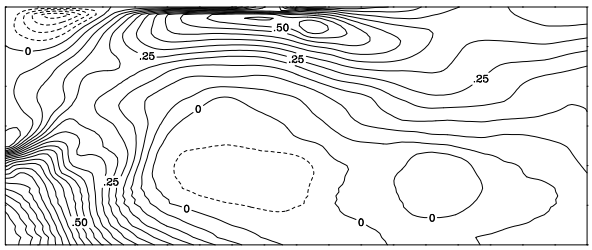

a) $\overline{U}/\mathrm{U}_0$

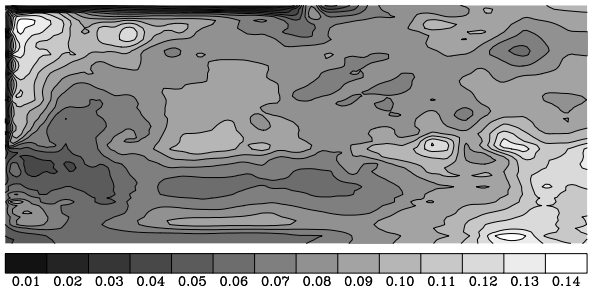

b) C_ν

Fig. 5 Two dimensional contour plot of (a) mean normalized axial velocity ($\overline{U}/\mathbf{U}_0$) and (b) mean eddy viscosity coefficient ($\mathbf{C}_\nu$). In (a), dashed lines denote negative velocities. X-axis ranges from $0 < x/D_0 < 3$**; Y-axis from** $0 < r/D_0 < 1.25$

The occurrence of a dominant frequency shared by these four variables leads to a strong coupling between the various modes of oscillation. The overall effect of these fluctuating modes is to drive strong flame-front oscillations (through both vortex-flame interaction and mass-flux oscillations). Unsteady shifts on the flame location correlate to heat-release oscillations (q'). As introduced previously, positive coupling of p' and q' can drive combustion instabilities. In Fig. 8, the time varying *Rayleigh Parameter* ($R(t)$), defined as $R(t) = \int\ p'\ q'\ \mathrm{d}V$, has been plotted along with the acoustic pressure. As can be seen, there are times during the simulation when $R(t)$ is positive indicating energy addition to the acoustic field.

5.3 Temporal equivalence ratio variation

As mentioned in the Introduction, a common source of instabilities is the interaction of longitudinal pressure oscillations and fuel feed-lines. This interaction leads to bulk temporal fluctuations in the incoming Φ. Modelling of this actual interaction will not be attempted in the study; however, a time variation on Φ has instead been studied. During the simulation, the inlet Φ is dropped from an elevated value of 0.62 down to 0.52. Previous studies[25] have shown that at higher equivalence ratios, the amplitude of p' is reduced.

Shown in Fig. 9 is the p' time trace and the analogous imposed inlet Φ. When Φ is elevated at 0.62, the peak-to-peak pressure fluctuations are within +/- 2% and the p' $rms \approx 1.0$. However, once Φ is dropped to 0.52, the peak-to-peak dramatically increases with a subsequent rms increase equal to that of the baseline simulation.

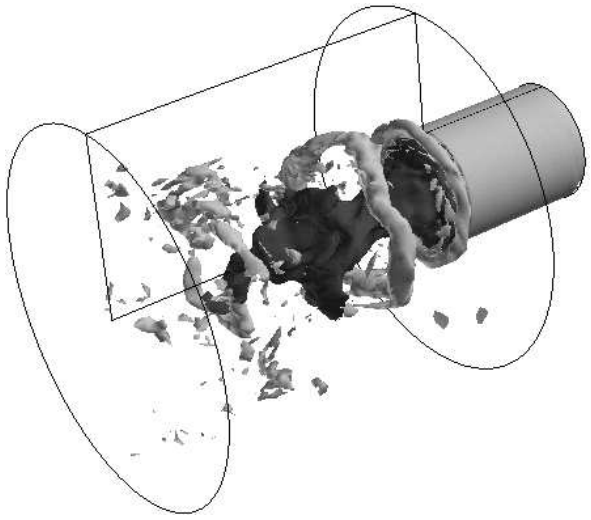

Fig. 6 Instantaneous vortex-flame interaction for baseline simulation. Grey iso-surface shows shead vortex rings emanating from the inlet boundary layer. Dark surface is the moving flame-front.

Of importance to active control system designers is the time delay or response time. In this situation, the response time is effected by both convection (i.e., the time to travel from the inlet to the flame region) and an acoustic time (i.e., the time for a wave to transfers the combustor). In this case, the response time, measured from the time at which Φ has dropped to its lowest value, is approximately 1.2 ms or 3.5 cycles if non-dimensionalized by the peak frequency. Based on the inlet mass flow rate and inlet length, the convective time is approximately 1/3 ms and is the same for resonant acoustic time. As can be seen, once the changes in Φ have reached the reaction zone, the acoustics respond quickly. In a similar study[26] in which the inlet swirl number is altered in time, the resulting time delay was much longer, requiring more then 15 cycles.

5.4 Spatial equivalence ratio variation

As a second use of the *partially-premixed* flamelet model, a non-uniform fuel concentration profile has been imposed at the combustor inlet. To allow for direct comparison, the total fuel flow-rate has been kept constant with that of the baseline study (overall $\Phi = 0.52$). The actual equivalence ratio profile has been plotted in Fig. 10.

The resulting p' time trace is shown in Fig. 11(a) along with that of the baseline simulation. Similar to the pressure fluctuations at higher Φ from the previous section, the peak-to-peak variations are much reduced compared to that of the baseline. The rms pressure is 1.09% compared to the baseline's 1.77% (a drop of 4 dB). Another deviation from the baseline is the peak

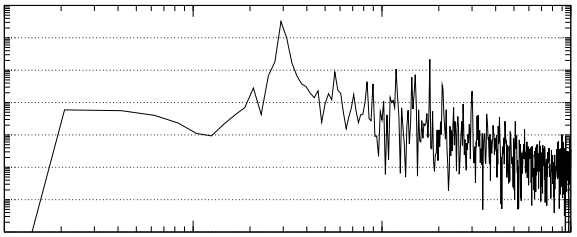

a) $\hat{p}(f)$

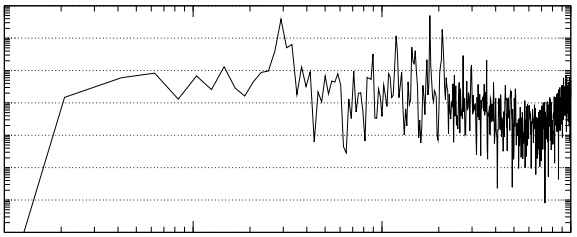

b) $\hat{\Delta}(f)$

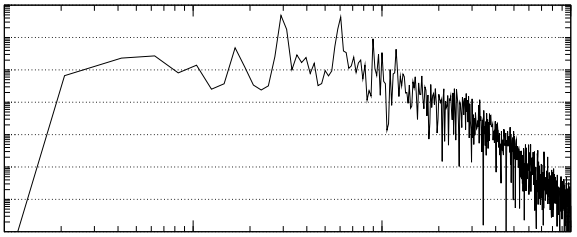

c) $|\hat{\omega}|(f)$

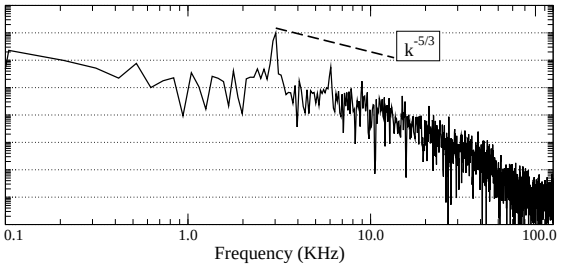

d) $\hat{u}(f)$

Fig. 7 Frequency spectra for fluctuating (a) pressure (p'), (b) divergence (Δ'), (c) vorticity magnitude ($|\omega|'$), and velocity (u'). Acoustic signals (i.e., Δ' and p') were recorded at the combustor base as noted in Fig. 2. Velocity signals ($|\omega|'$ and u') were recorded in the swirling shear-layer at r / D_0 = 0.6 and 1.1 D_0 downstream from the combustor base plane.

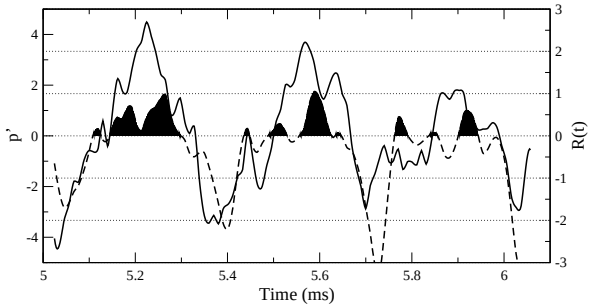

Fig. 8 Shown here are the unsteady Rayleigh parameter ($R(t)$) and fluctuating pressure p' through a short time window. $R(t)$ is plotted with dashed line (- - -) and p' with solid line. To clarify acoustic energy amplification, $|p'\ q'| > 0$, those regions have been filled with black.

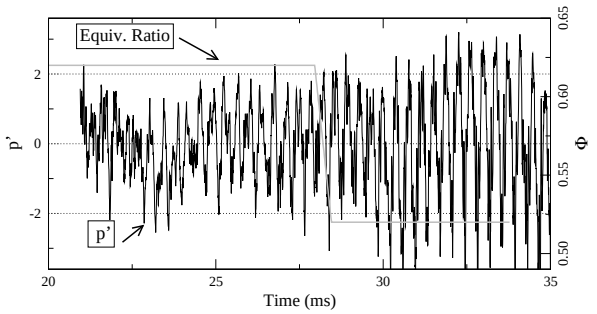

a) $p'(t)$

Fig. 9 Fluctuating pressure (p') and equivalence ratio (Φ) through time for temporal Φ variation simulation. Φ is shown with symbols while p' is shown with a black line.

frequency (see Fig. 11) which has shifted by 160 Hz from 2918 to 3079 Hz. A possible cause of this difference is in the variation in combustor temperature as a result of the fluctuations in the local equivalence ratio.

Despite the highly turbulent flow issuing from the swirling inlet, large differences in Φ still persist through the flame-front/heat-release zone. This effect is shown in Fig. 12(a) were the time-averaged rms equivalence ratio (Φ') has been plotted through a slice of the combustor. As can be seen from this figure, the bulk of equivalence ratio fluctuations are located downstream beyond the combustor base plane and into the combustion zone. This unmixedness also leads to a lengthened flame compared to the baseline. Fig. 12(b) shows the time-averaged product temperature ($\overline{T_f}$). Downstream and away from the flame, temperature gradients still exists. The higher temperatures are located towards the outer edges of the combustor due to the longer residence times in these regions (increased thermal mixing). Also, as a result of the inlet Φ profile, more thermal energy is contained in the fluid away from the centerline. This fluid is then entrained in the shear-layer and behind the ex-

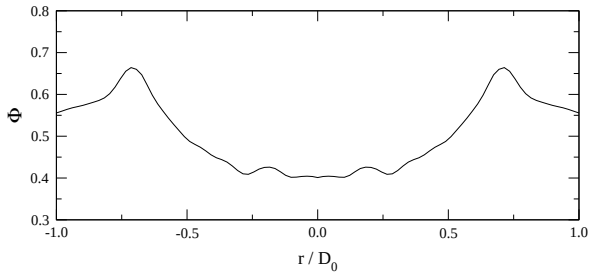

Fig. 10 Inlet fuel concentration profile for spatial equivalence ratio variation study. The profile is scaled so as to maintain the same overall equivalence ratio as baseline study ($\Phi = 0.52$).

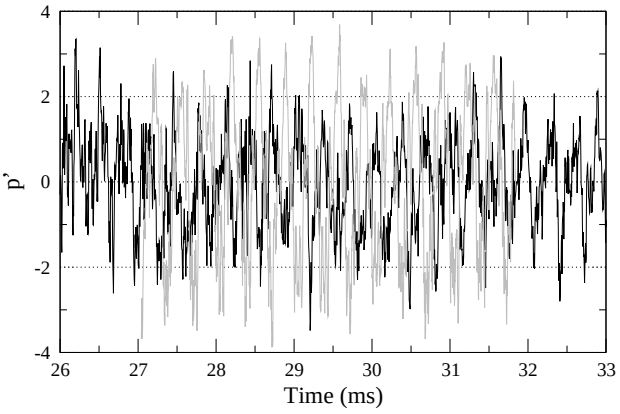

a) $p'(t)$

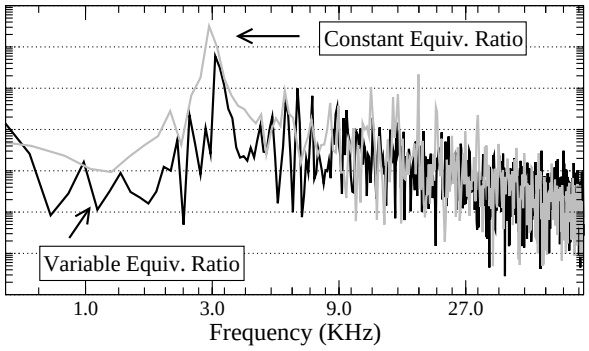

b) $\hat{p}(f)$

Fig. 11 Fluctuating pressure (a) (p') time trace and (b) ($\hat{p}(f)$) frequency spectrum for spatial Φ variation simulation.

pansion wall while the lower-energy jet core is more readily convected downstream. Further downstream, the temperature becomes more uniform due to turbulent mixing and conduction.

6 Conclusions

In this is paper, the effects of equivalence ratio variations on combustion dynamics in an idealized gas turbine combustor have been studied. Large-Eddy Simulation (LES) was used to numerically model the

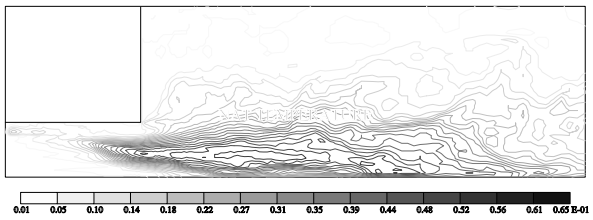

a) $\Phi'(x)$

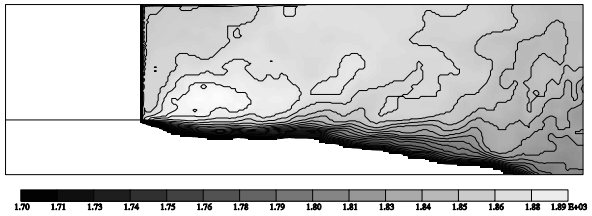

b) $\overline{T_f}(x)$

Fig. 12 Plotted here are the time-averaged (a) equivalence ratio rms (Φ') and (b) product temperature ($\overline{T_f}$) for case 3.

three-dimensional turbulent combustion processes. A *partially-premixed* combustion model was employed to account for the variations in the local equivalence ratio at only a minimal cost increase. Validation of the premixed combustion model was also given before analysis of the present work.

Three simulations were presented and their results discussed and analyzed. The first case, with constant equivalence ratio, was used as a baseline for the later two. In this case, the longitudinal pressure fluctuations were shown to be significant and coupled with other modes of oscillation (vortex-shedding). The velocity energy spectrum was also analyzed, showing the resolution into the inertial length-scale range.

The *partially-premixed* combustion model was employed for two different situations. The first test was to model temporal variations in the inlet equivalence ratio. This case was used to test the combustion model's ability to simulate the interaction of pressure oscillations with fuel feed-lines. It was shown that the pressure fluctuations respond quite rapidly to changes in the inlet equivalence ratio. It was observed that only 3.5 oscillation cycles were needed to fully respond to the inlet changes. Finally, the combustion model was used to model spatial variations (unmixedness) issuing from the swirling premixer. It was found that, in this case, the combustion instabilities were suppressed, by as much as 4 dB over the baseline case, as a result of the downstream product temperature gradients.

7 Acknowledgments

This work was supported in part by the Army Research Office (ARO), Wright-Patterson AFB, and General Electric Power Systems. High Performance

Computing (HPC) resources were provided by the Department of Defense Major Shared Resources Centers at the Naval Oceanographic Office (NAVOCEANO), Aeronautical Systems Center (ASC), Army Engineering Research and Development Center (ERDC), and Army Research Laboratory (ARL) under HPC Grand Challenge projects from the Army Research Office and Wright-Patterson AFB.

References

[1] Joshi, N. D., Mongia, H. C., Leonard, G., Stegmaier, J. W., and Vickers, E. C., "Dry Low Emissions Combustor Development," *ASME Paper 98GT-310*, 1998.

[2] Paschereit, C., Gutmark, E., and Weisenstein, W. W., "Coherent structures in swirling flows and their role in acoustic combustion control," *Physics of Fluids*, Vol. 11, 1999, pp. 2667–2678.

[3] Kim, W.-W. and Menon, S., "Numerical modeling of turbulent premixed flames in the thin-reaction-zones regime," *Combustion Science and Technology*, Vol. 160, 2000, pp. 110–150.

[4] Stone, C. and Menon, S., "Parallel Simulations of Swirling Turbulent Flames," *Journal of Supercomputing*, Vol. 22, No. 1, 2002, pp. 7–28.

[5] Yang, V. and Culick, F. E., "Analysis of low frequency combustion instabilities in a laboratory ramjet combustor," *Combustion Science and Technology*, Vol. 45, 1986, pp. 1–25.

[6] Lieuwen, T. and Zinn, B. T., "The Role of Equivalence Ratio Oscillations in Driving Combustion Instabilities in Low NOx Gas Turbines," *Proceedings of the 27th International Symposium on Combustion*, 1998, pp. 1809–1816.

[7] Lieuwen, T., Torres, H., Johnson, C., and Zinn, B. T., "A Mechanism for Combustion Instabilities in Premixed Gas Turbine Combustors," *Journal of Engineering for Gas Turbines and Power*, Vol. 123, 2001, pp. 182–189.

[8] Erlebacher, G., Hussaini, M. Y., Speziale, C. G., and Zang, T. A., "Toward the Large-Eddy Simulation of Compressible Turbulent Flows," *Journal of Fluid Mechanics*, Vol. 238, 1992, pp. 155–185.

[9] Menon, S., Yeung, P.-K., and Kim, W.-W., "Effect of Subgrid Models on the Computed Interscale Energy Transfer in Isotropic Turbulence," *Computers and Fluids*, Vol. 25, No. 2, 1996, pp. 165–180.

[10] Chakravathy, V. K. and Menon, S., "Subgrid Modeling of Turbulent Premixed Flames in the Flamelet Regime," *Flow, Turbulence and Combustion*, Vol. 5, 2000, pp. 23–45.

[11] Kim, W.-W., Menon, S., and Mongia, H. C., "Large eddy simulations of a gas turbine combustor flow," *Combustion Science and Technology*, Vol. 143, 1999, pp. 25–62.

[12] Peters, N., *Turbulent Combustion*, Cambridge University Press, 2000.

[13] Williams, F. A., *Combustion Theory*, Benjamin/Cummins, 1985.

[14] Kerstein, A. R., Ashurst, W. T., and Williams, F. A., "The field equation for interface propagation in an unsteady homogeneous flow field," *Physical Review A*, Vol. 37, 1988, pp. 2728–2731.

[15] Smith, T. M. and Menon, S., "The structure of premixed flames in a spatially evolving turbulent flow," *Combustion Science and Technology*, Vol. 119, 1996, pp. 77–106.

[16] Pocheau, A., "Scale invariance in turbulent front propagation," *Physical Review E*, Vol. 49, 1994, pp. 1109–1122.

[17] Kee, R. J., Grcar, J. F., Smooke, M. D., and Miller, J. A., "A Fortran program for modeling steady laminar one-dimensional premixed flames," *Sandia Report SAND85-8240, Sandia National Labs., Livermore, CA.*, 1993.

[18] Kee, R. J., Rupley, F. M., and Miller, J. A., "Chemkin-II: A Fortran chemical kinetics package for the analysis of gas phase chemical kinetics," *Sandia Report SAND89-8009B, Sandia National Labs., Livermore, CA.*, 1993.

[19] MacCormack, R. W., "The effects of viscosity in hypervelocity impact cratering," *AIAA Paper 69–354*, 1969.

[20] Gottlieb, D. and Turkel, E., "Dissipative two-four methods for time-dependent problems," *Mathematics of Computation*, Vol. 30, No. 136, 1976, pp. 703–723.

[21] Poinsot, T. and Lele, S., "Boundary conditions for direct simulations of compressible viscous flow," *Journal of Computational Physics*, Vol. 101, 1992, pp. 104–129.

[22] Escudier, M. P. and Keller, J. J., "Recirculation in swirling flow: a manifestation of vortex breakdown," *AIAA Journal*, Vol. 23, No. 111, 1985.

[23] Jeong, J. and Hussain, F., "On the Identification of a Vortex," *Journal of Fluid Mechanics*, Vol. 285, 1995, pp. 69–94.

[24] Ducruix, S., Durox, D., and Candel, S., "Theoritical and Experimental Determinations of the Transfer Function of a Laminar Premixed Flame," *Proceedings of the Combustion Institute*, Vol. 28, 2000, pp. 765–773.

[25] Stone, C. and Menon, S., "Combustion instabilities in swirling flows," *37th AIAA/ASME/SAE/ASEE Joint Propulsion Conference, AIAA 2001-3846*, 2001.

[26] Stone, C. and Menon, S., "Adaptive Swirl Control of Combustion Dynamics in Gas Turbine Combustors," *Proceedings of the 29th International Symposium on Combustion (to appear)*, 2002.